Environmental Pollution 258 (2020) 113703

Contents lists available at ScienceDirect

Environmental Pollution

journal homepage: www.elsevier.com/locate/envpol

Microbial degradation kinetics and molecular mechanism of 2,6-dichloro-4-nitrophenol by a *Cupriavidus* strain☆

Jun Min [a, b, c], Lingxue Xu [a, d], Suyun Fang [a, b], Weiwei Chen [a, b], Xiaoke Hu [a, b, c, *]

[a] Key Laboratory of Coastal Biology and Bioresource Utilization, Yantai Institute of Coastal Zone Research, Chinese Academy of Sciences, Yantai, China
[b] Laboratory for Marine Biology and Biotechnology, Qingdao National Laboratory for Marine Science and Technology, Qingdao, China
[c] Center for Ocean Mega-Science, Chinese Academy of Sciences, Qingdao, China
[d] College of Life Science of Yantai University, Yantai, China

ARTICLE INFO

Article history:
Received 8 July 2019
Received in revised form
3 November 2019
Accepted 29 November 2019
Available online 30 November 2019

Keywords:
2,6-Dichloro-4-nitrophenol
Biodegradation kinetics
Microbial degradation mechanism
Evolutionary origin
Two-component monooxygenase

ABSTRACT

2,6-Dichloro-4-nitrophenol (2,6-DCNP) is an emerging chlorinated nitroaromatic pollutant, and its fate in the environment is an important question. However, microorganisms with the ability to utilize 2,6-DCNP have not been reported. In this study, *Cupriavidus* sp. CNP-8 having been previously reported to degrade various halogenated nitrophenols, was verified to be also capable of degrading 2,6-DCNP. Biodegradation kinetics assay showed that it degraded 2,6-DCNP with the specific growth rate of 0.124 h^{-1}, half saturation constant of 0.038 mM and inhibition constant of 0.42 mM. Real-time quantitative PCR analyses indicated that the *hnp* gene cluster was involved in the catabolism of 2,6-DCNP. The *hnpA* and *hnpB* gene products were purified to homogeneity by Ni-NTA chromatography. Enzymatic assays showed that HnpAB, a FAD-dependent two-component monooxygenase, converted 2,6-DCNP to 6-chlorohydroxyquinol with a K_m of 3.9 ± 1.4 μM and a k_{cat}/K_m of 0.12 ± 0.04 μM^{-1} min^{-1}. As the oxygenase component encoding gene, *hnpA* is necessary for CNP-8 to grow on 2,6-DCNP by gene knockout and complementation. The phylogenetic analysis showed that the *hnp* cluster originated from the cluster involved in the catabolism of chlorophenols rather than nitrophenols. To our knowledge, CNP-8 is the first bacterium with the ability to utilize 2,6-DCNP, and this study fills a gap in the microbial degradation mechanism of this pollutant at the molecular, biochemical and genetic levels. Moreover, strain CNP-8 could degrade three chlorinated nitrophenols rapidly from the synthetic wastewater, indicating its potential in the bioremediation of chlorinated nitrophenols polluted environments.

1. Introduction

As the most common halogenated nitroaromatic compounds, chlorinated nitrophenols (CNPs) have been extensively used as intermediates in synthesis of various industrial chemicals (Arora et al., 2018). CNPs are severe environmental pollutants, being potentially hazardous to human health and animals (Arora et al., 2012a,b). 2,6-Dichloro-4-nitrophenol (2,6-DCNP) is a typical representative of CNPs, and it is released into the environment during its manufacture, transport and application. Also, it is a common halogenated disinfection by-product and has been detected in various water environments (Xiao et al., 2012; Jiang et al., 2017; Liu et al., 2019). The toxicological studies have demonstrated that 2,6-DCNP is more toxic compared to many regulated disinfection by-products by the U.S. EPA (Yang and Zhang, 2013; Liu and Zhang, 2014). Thus, removal of this pollutant is very significant due to its toxic profiles and its widespread occurrence throughout the environment.

Both physical and chemical methods have been applied to treat CNPs-contaminated water; however, these solutions are unable to degrade the pollutants completely (Arora et al., 2012a,b; Arora et al., 2018). In contrast, biological degradation is considered as a promising approach to clean up contamination in the environment. Previously, bioremediation has been successfully applied in remediating various environments contaminated by aromatic compounds (Cunliffe and Kertesz, 2006; Niu et al., 2009; Dastgheib et al., 2012; Chi et al., 2013; Wang et al., 2014; Fu et al., 2017; Min et al., 2017a; Yue et al., 2018). However, it is well known that the

☆ This paper has been recommended for acceptance by Dr. Jörg Rinklebe.

* Corresponding author. Key Laboratory of Coastal Biology and Bioresource Utilization, Yantai Institute of Coastal Zone Research, Chinese Academy of Sciences, Yantai, China.

E-mail address: xkhu@yic.ac.cn (X. Hu).

https://doi.org/10.1016/j.envpol.2019.113703
0269-7491/

essential prerequisite for bioremediation is to obtain a single microorganism or a consortium with the ability to degrade the target pollutant.

Up to now, studies on microbial degradation of CNPs by pure culture bacteria were mainly focused on monochlorinated nitrophenols. Many bacteria with the ability to degrade monochlorinated nitrophenols such as 2-chloro-4-nitrophenol (2C4NP) (Ghosh et al., 2010; Arora and Jain, 2011; Pandey et al., 2011; Arora and Jain, 2012; Min et al., 2014; Min et al., 2016; Tiwari et al., 2017), 2-chloro-5-nitrophenol (2C5NP) (Schenzle et al., 1999; Min et al., 2017b), 4-chloro-2-nitrophenol (Arora et al., 2012a,b) or 4-chloro-3-nitrophenol (Arora et al., 2014) have been isolated. Due to the different substitutional position of chloro and nitro groups on the aromatic ring, these bacteria exhibited various catabolic pathways against different isomers (Arora et al., 2018). However, in contrast to monochlorinated nitrophenols, dichlorinated nitrophenols (DCNP) such as 2,6-DCNP and its isomers are more toxic and more resistant to microbial degradation due to the extra chlorine substituent on the aromatic ring. Thus, no microorganism has been reported to utilize 2,6-DCNP to date, although it was detected as a serious pollutant in the environment.

Therefore, our objective is to identify a microorganism with the ability to degrade 2,6-DCNP and investigate the microbial degradation of this pollutant, providing a foundation for bioremediation. Initially, we aimed to isolate bacteria that can utilize 2,6-DCNP as the sole source of carbon but failed after several attempts. Previously, *Cupriavidus* sp. strain CNP-8 isolated by us has been reported to degrade several nitrophenols including *meta*-nitrophenol (MNP) and 2C5NP (Min et al., 2017b), 2C4NP (Min et al., 2018) and 2,6-dibromo-4-nitrophenol (2,6-DBNP) (Min et al., 2019). Moreover, it degraded (halogenated)-*meta*-nitrophenol (such as MNP and 2C5NP) via the partial reductive pathways, whereas degraded halogenated *para*-nitrophenols (such as 2C4NP and 2,6-DBNP) via the oxidative pathways. Thus, given the ability of strain CNP-8 to degrade various halogenated nitrophenols, it was employed to see if it could also utilize 2,6-DCNP.

In our investigation, strain CNP-8 turned out to indeed use 2,6-DCNP as the sole source of carbon and nitrogen. We investigate the biodegradation kinetics of 2,6-DCNP by this strain. Moreover, the catabolic pathway of 2,6-DCNP was characterized from the perspective on molecular biology and biochemistry. The evolutionary origin of HnpA which initiates the catabolism of 2,6-DCNP was revealed by phylogenetic analysis. This study fills a gap in the knowledge of microbial degradation of 2,6-DCNP and enhances our understanding of the evolutionary origin of the enzymes involved in nitrophenols catabolism.

2. Materials and methods

2.1. Biodegradation experiments

Cupriavidus sp. strain CNP-8 employed in current study was isolated previously by us from the pesticide-contaminated soil in Yantai, China (Min et al., 2017b), and it has been deposited in the China Center for Type Culture Collection (CCTCC No. M 2017546). In this study, to investigate the ability of *Cupriavidus* sp. CNP-8 to utilize 2,6-DCNP, this strain was grown in minimal medium (Liu et al., 2005) (MM, without $CaCl_2$, pH = 7.0) supplemented with 2,6-DCNP as the sole carbon and nitrogen source. This aerobic biodegradation experiments were carried out in 250 ml Erlenmeyer flasks containing 100 ml MM with 0.4 mM 2,6-DCNP. Before the experiment, strain CNP-8 was initially cultivated overnight in MM + lysogeny broth (LB) (4:1, *v/v*) containing 0.4 mM of 2,6-DCNP. The cells were harvested, washed twice and resuspended in fresh MM. Then, the cells suspension was inoculated in 100 ml MM (with 0.4 mM 2,6-DCNP) at initial OD_{600} of 0.05, and the flasks were shaken at 180 rpm at 30 °C. The ability of strain CNP-8 to utilize 2,6-DCNP was determined by measuring the bacterial growth (OD_{600}) and substrate's consumption, together with nitrite and chlorine ions release. To investigate the potential of strain CNP-8 in biotreatment of CNPs-contaminated wastewater, aerobic biodegradation of three CNPs by this strain was carried out in 4 L batch reactors containing 2 L synthetic wastewater (Ahmadi et al., 2015), which contains 2C4NP, 2C5NP and 2,6-DCNP (the concentration of each CNP is 0.3 mM). Strain CNP-8 was initially cultivated overnight in LB medium and washed twice by synthetic wastewater before being introduced into the reactors at a concentration of 5×10^7 cells per liter. The reactors were operated at room temperature and continuously aerated using an air-compressing pump at a flow rate of 250 ml min^{-1}. The samples were withdrawn regularly, centrifuged (13,000×*g*, 10 min), and the concentrations of CNP in the supernatant were assayed by HPLC.

2.2. Biodegradation kinetics of 2,6-DCNP

To study the biodegradation kinetics of 2,6-DCNP, the effect of different initial concentrations of substrate (0.05–1.5 mM) on bacterial growth was investigated. In current study, the aeration provided by shaking the flasks is able to keep the oxygen concentration sufficient. Therefore, the strain CNP-8 growth rate and 2,6-DCNP degradation rate were only limited by substrate concentration at fixed initial temperature (30 °C), pH (7.0) and shaking rate (180 rpm).

Bacterial growth kinetics can be modeled by the following equation

$$\ln(X/X_0) = \mu t \tag{1}$$

The dry weight of biomass of strain CNP-8 was converted from the OD_{600} value using a standard curve [dry weight (mg/L) = $564.7 \times OD_{600} - 2.75$, $R^2 = 0.986$] (Min et al., 2018).

Because of the inhibition effect of 2,6-DCNP for CNP-8, Haldane's model (Wang et al., 2010) was used to investigate the kinetics of 2,6-DCNP biodegradation. The equation of the Haldane model was described as follow:

$$\mu = \frac{\mu\text{max}S}{Ks + S + (S^2 / Ki)} \tag{2}$$

where S is the substrate concentration (mg L^{-1}), μ_{max} is the maximum specific growth rate (h^{-1}), K_s is the half saturation constant (mg L^{-1}), K_i is the inhibition constant (mg L^{-1}).

For 2,6-DCNP degradation, the specific degradation rate was defined as follows (Sun et al., 2016):

$$q = -\frac{1}{X}\frac{dS}{dt} \tag{3}$$

The maximum specific degradation rate obtained by Haldane's model as follows (Sun et al., 2016):

$$q = \frac{q_{max}\, S}{S + K_S + (S^2 / K_i)} \tag{4}$$

where S is the substrate concentration; q is the specific degradation rate; q_{max} is the maximum specific degradation rate.

The biomass was estimated by the following equation (Min et al., 2018):

$$Y = \frac{X - X0}{S0 - S} \tag{5}$$

where X_{max} is the maximum biomass (mg L^{-1}), X_0 is the initial biomass, S_0 is the initial substrate concentration (mg L^{-1}), S_a is the substrate concentration when the biomass is maximum.

2.3. Biotransformation assay

The biotransformation assays were performed as described (Chen et al., 2014) with little modification. Briefly, CNP-8 was grown on MM with 20% LB to an OD_{600} of 0.2, followed by substrate (2,6-DCNP or 2,6-DBNP) induction for 6 h. The harvested cells were washed twice and suspended to OD_{600} of 2 in phosphate buffer (20 mM, pH 7.2), followed by addition of 0.4 mM substrate. The groups with no addition of substrate were used as uninduced control. Samples (1 ml) were taken at 10-min intervals and centrifuged 10 min at 13,000×*g* at 4 °C. The concentrations of halogenated nitrophenols were determined by HPLC.

2.4. Real-time quantitative PCR (RT-qPCR) analysis

The total RNA of the 2,6-DCNP-induced and uninduced cells of strain CNP-8 was isolated and reverse transcribed as described (Min et al., 2017b). RT-qPCR was carried out on a 7500 fast real-time PCR system with the primers listed in Table S1. The transcriptional levels of the target genes were calculated by the $2^{-\Delta\Delta C_T}$ method (Livak and Schmittgen, 2001) with 16S rRNA gene as control.

2.5. Protein purification and enzymatic assays

hnpA and *hnpB* were respectively cloned into the *Nde*I/*Xho*I digested vector pET28a, and the N-terminal His-tagged HnpA and HnpB were over-expressed in *E. coli* BL21(DE3) and purified (Min et al., 2019). The Bradford method (Bradford, 1976) was used to determine the protein concentrations. The enzymatic assays of HnpAB against 2,6-DCNP was performed using a UV/Vis spectrophotometer (PE Lambda 365). The reaction system (1 ml) contained Tris-HCl buffer (pH 7.5), 30 μg HnpA, 5 μg HnpB, 20 μM FAD and 200 μM NADH, and the reaction was initiated by substrate addition. In the case of the kinetics assays, the concentrations of 2,6-DCNP range from 0.5 to 40 μM with FAD and NADH fixed concentration (0.02 mM and 0.2 mM, respectively). For the products' identification, the reaction products generated from 2,6-DCNP after incubations with HnpAB were acetylated, dried over sodium sulfate and analyzed by gas chromatography-mass spectrometry (GC-MS).

2.6. Analytical methods

The CNP compounds were analysis by HPLC with an Agilent XDB-C18 column (250 mm × 4.6 mm × 5 μm) and detected by a DAD detector at 320 nm. The mobile phase was the same as described (Min et al., 2019). GC-MS analysis was carried out on a Thermo Trace GC Ultra gas chromatograph equipped with an Agilent HP-5MS capillary column (30 m × 0.25 mm, 0.25 μm) and coupled with an ITQ 900 ion trap mass spectrometer (Thermo Scientific). The condition of GC-MS analysis was the same as described (Min et al., 2016). An ion-selective combination chloride electrode (Model 96-17, Orion) was used to detect the chlorine ion. The concentrations of nitrite were determined by colorimetric method (Lessner et al., 2002).

2.7. Phylogenetic analysis

The phylogenetic tree for HnpA and the oxygenase components of other two-component aromatic monooxygenases was constructed using the neighbor-joining method by the MEGA 5.02 software (Tamura et al., 2011). The topologic accuracy of the tree was evaluated by using 1000 bootstrap replicates.

3. Results

3.1. Strain CNP-8 can grows on 2,6-DCNP

The degradation of 2,6-DCNP by strain CNP-8 was determined on MM supplemented with 0.4 mM 2,6-DCNP as the sole source of carbon and nitrogen. As shown in Figs. 1 and 2,6-DCNP was completely degraded within 35 h. Meanwhile, the cell density increased gradually, together with nitrite and chlorine ions accumulation. The accumulation of nitrite proposed that strain CNP-8 degraded the substrate via oxidative denitration. 0.76 mM chlorine ion was accumulated when 2,6-DCNP was completely degraded, indicating that strain CNP-8 can remove two chlorines from 2,6-DCNP. Conversely, neither 2,6-DCNP degradation nor bacterial growth was observed in a control without CNP-8 inoculation. To our knowledge, strain CNP-8 is the first microbe capable of utilizing 2,6-DCNP, which motivated us to carry out the subsequent work.

3.2. Biodegradation kinetic of 2,6-DCNP

Biodegradation of 2,6-DCNP at different concentrations was investigated to estimate the effect of 2,6-DCNP's concentration on CNP-8's growth. As shown in Fig. S1, the added 2,6-DCNP was degraded completely while the concentration of 2,6-DCNP was no more than 1 mM. Meanwhile, the delay periods of substrate degradation and cell growth extended significantly with 2,6-DCNP concentration increase. Neither 2,6-DCNP degradation nor bacterial growth occurred when initial 2,6-DCNP was increased up to 1.5 mM.

The biodegradation assay indicated that high concentration 2,6-DCNP could inhibite the growth of strain CNP-8. Therefore,

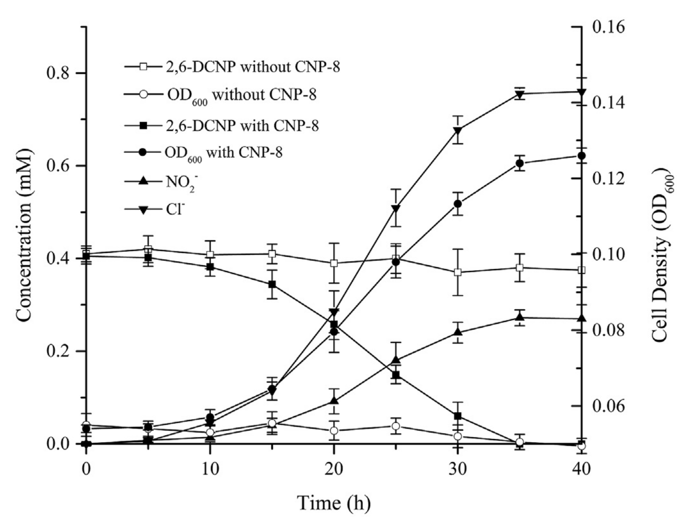

Fig. 1. Time course of 2,6-DCNP degradation by *Cupriavidus* sp. strain CNP-8 in mineral salts medium, together with the accumulation of NO_2^-, Cl^- and OD_{600}. (■) 2,6-DCNP concentration with strain CNP-8 inoculation; (□) 2,6-DCNP concentration without strain CNP-8 inoculation; (●) OD_{600} with 2,6-DCNP addition; (○) OD_{600} without 2,6-DCNP addition; (▲) NO_2^- (▼) Cl^-.

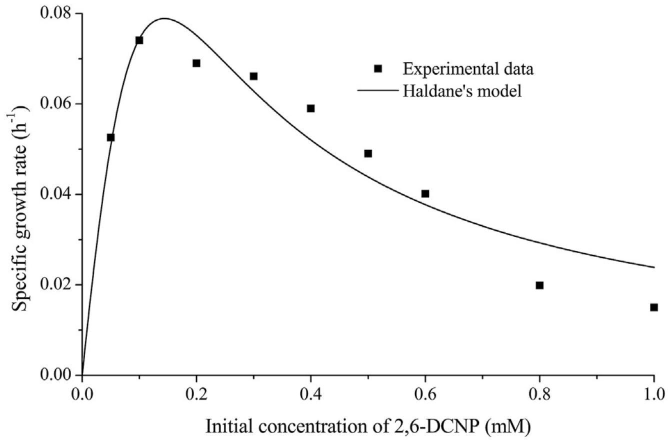

Fig. 2. Experimental and predicted specific growth rates of strain CNP-8 against 2,6-DCNP according to Haldane's model.

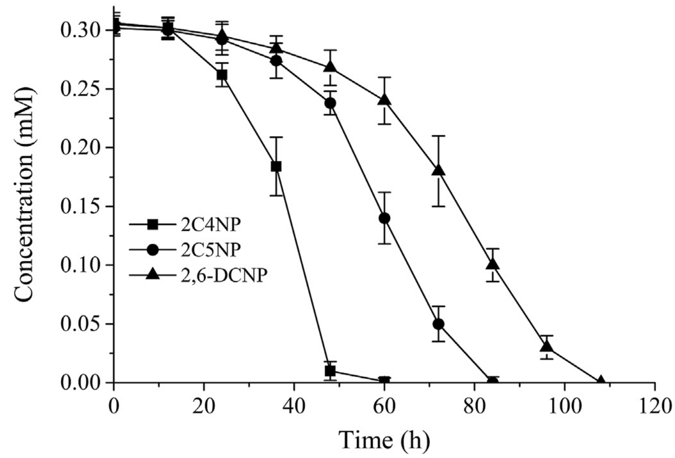

Fig. 3. Simultaneous degradation of three chlorinated nitrophenols by strain CNP-8 from the synthetic wastewater. (■) 2C4NP; (● 2C5NP; (▲) 2,6-DCNP.

Haldane's growth kinetics model was used to estimate the kinetic parameters of microbial 2,6-DCNP degradation. Non-linear regression analysis of the bacterial growth data (Fig. S1) was performed using Origin software (Version 8.0). Experimental and predicted specific growth rates of strain CNP-8 due to Haldane's model were shown in Fig. 2. The kinetic parameters for CNP-8's growth on 2,6-DCNP obtained by Eq. (2), and μ_{max} (the maximum specific growth rate) = 0.124 h^{-1}, K_s (half saturation constant) = 0.038 mM, K_i (inhibition constant) = 0.42 mM (R^2 = 0.927, standard deviation = 0.086). The value of μ_{max} increased with the initial 2,6-DCNP increasing to about 0.13 mM, and then declined on further increasing substrate concentration. Similarly, for substrate degradation, the specific degradation rates (q) increased with increase of initial 2,6-DCNP concentration, and then declined on further increasing substrate concentration (Fig. S2). The maximum specific degradation rate (q_{max}) was obtained by Eq. (4). By non-linear regression analysis using Origin software, q_{max} was obtained as mg substrate mg^{-1} biomass h^{-1}.

The biomass yield coefficient (mg dry weight of biomass mg^{-1} substrate) was estimated by linearizing biomass increase with 2,6-DCNP consumption, as estimated by Eq. (5). The biomass yield coefficient varied from 0.06 mg mg^{-1} to a maximum of 0.29 mg mg^{-1} (Fig. S3). The yield coefficient varied slightly when 2,6-DCNP concentrations was no more than 0.3 mM. However, the yield coefficient declined apparently when the initial substrate concentrations were further increased up to 1 mM.

3.3. Simultaneous degradation of three CNPs from synthetic wastewater by strain CNP-8

In addition to degrading 2,6-DCNP, strain CNP-8 has been previously proved to be capable for utilizing two monochlorinated nitrophenols including 2C4NP (Min et al., 2018) and 2C5NP (Min et al., 2017a,b). These three chlorinated nitrophenols would coexist in the industrial wastewater due to their extensive uses in the synthesis of various industrial chemicals (Arora et al., 2018). So, simultaneous degradation of the three pollutants by strain CNP-8 was performed to investigate its potential in bioremediation. As shown in Fig. 3, although all three CNPs at 0.3 mM could be degraded completely from the synthetic wastewater, different degradation rates were observed among them. 2C4NP was completely removed in the first 48 h; however, 79% (0.238 ± 0.015 mM) of 2C5NP and 88% (0.267 ± 0.024 mM) of 2,6-DCNP remained after this period. The complete degradation of 2C5NP and 2,6-DCNP occurred in 84 h and 108 h, respectively. Although 2C4NP and 2C5NP are isomers, the degradation rate of 2C4NP is significantly faster than that of 2C5NP, indicating that the latter is more difficult to degrade by CNP-8 than the former. The degradation rate of 2,6-DCNP is significantly low as compared to other two mono-chlorinated nitrophenols. This is due to that 2,6-DCNP with an extra chloro on the aromatic ring is more toxic and more resistant to microbial degradation (Arora et al., 2018). This speculation can be furter justified by comparing the kinetic parameters of 2,6-DCNP with those of 2C4NP. Previously, strain CNP-8 has been reported to degrade 2C4NP as high as 1.6 mM, with K_s of 0.022 mM and K_i of 0.72 mM (Min et al., 2018). In this study, this strain utilized 2,6-DCNP less than 1.0 mM, with K_s of 0.038 mM and K_i of 0.42 mM. These combined data indicated that strain CNP-8 had lower substrate affinity for 2,6-DCNP, and higher inhibition by 2,6-DCNP as compared to 2C4NP. Thus, 2C4NP was removed faster than 2,6-DCNP. On the other hand, considering that strain CNP-8 is able to utilize 2C4NP, 2C5NP and 2,6-DCNP, respectively, as the sole source of carbon and nitrogen, and no intermediates should accumulate in the environment after completion of the biodegradation process; therefore, strain CNP-8 could be a promising candidate for the bioremediation of 2C4NP-contaminated sites.

3.4. The hnp gene cluster is involved in 2,6-DCNP catabolism

Previously, strain CNP-8 has been reported to degrade 2,6-dibromo-4-nitrophenol (2,6-DBNP, the brominated analogue of 2,6-DCNP) by the enzymes encoded by the *hnp* genes (Min et al., 2019). So, biotransformation assays were carried out to investigate where the catabolism of these two halogenated nitrophenols share the same enzymes. The uninduced cells of strain CNP-8 showed undetectable activity against both halogenated nitrophenols. However, either 2,6-DBNP- or 2,6-DCNP-induced cells of strain CNP-8 have the ability to degrade both halogenated nitrophenols rapidly (Fig. 4). This indicated that the catabolism of 2,6-DCNP in CNP-8 was performed by the enzymes encoded by the *hnp* gene cluster (GenBank accession number: MH271067), as outlined and annotated in Fig. 5A. Indeed, further transcription level analysis showed that the transcription levels of *hnpA*, *hnpB*, *hnpC* and *hnpD* in 2,6-DCNP-induced cells of strain CNP-8 increased 330-, 202-, 172- and 43-fold, respectively (Fig. 5B), significantly higher compared to those in the uninduced cell.

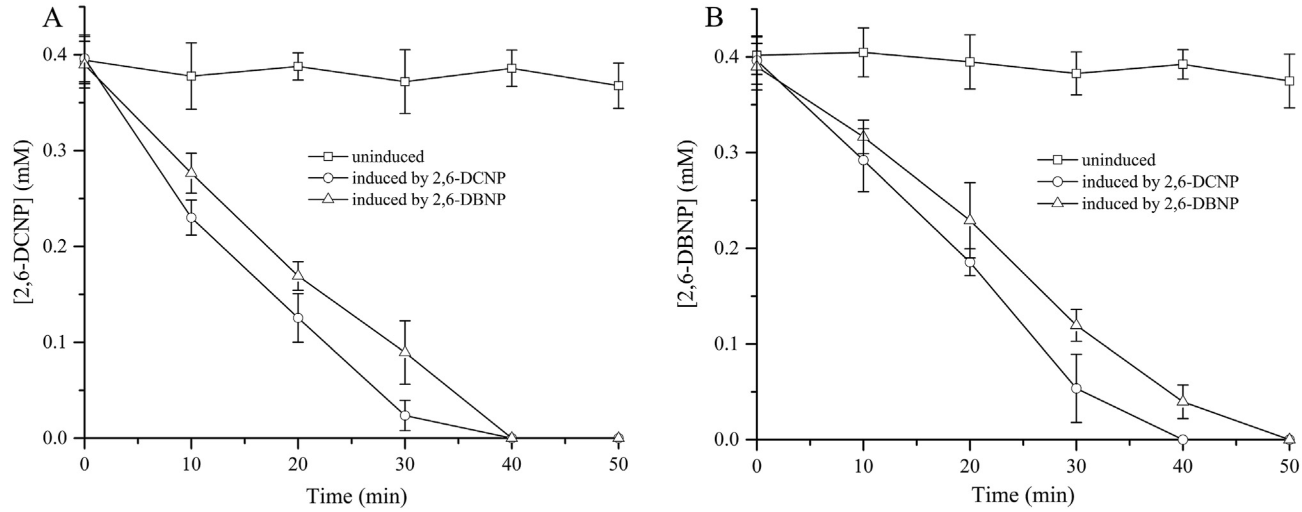

Fig. 4. Biotransformation of 2,6-DCNP **(A)** and 2,6-DBNP **(B)** by the induced and uninduced cells of strain CNP-8. (□) uninduced cells; (○) 2,6-DCNP-induced cells; (△) 2,6-DBNP-induced cells.

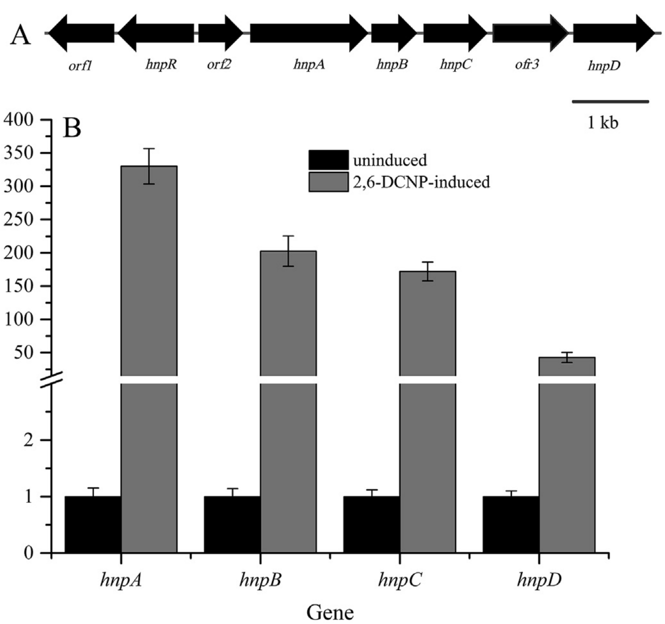

Fig. 5. Analysis of *hnp* gene cluster of strain CNP-8. (A) Schematic of the *hnp* gene cluster. The black arrows indicate the sizes and orientation of transcribed genes. (B) Transcriptional analyses of *hnpA*, *hnpB*, *hnpC* and *hnpD* in strain CNP-8 under induced and uninduced conditions by RT-qPCR.

3.5. Enzymatic assays of purified HnpAB against 2,6-DCNP

To further confirm whether *hnpAB* is involved in the catabolism of 2,6-DCNP, their products were expressed and purified, respectively (Fig. S4). As shown as in Fig. 6A, the two-component HnpA (the oxygenase component) B (the reductase component) degrades 2,6-DCNP (λ_{max} = 400 nm) rapidly, together with NADH (λ_{max} = 340 nm) consumption. In contrast, neither 2,6-DCNP nor NADH consumption was found when purified HnpB was omitted from the reaction system (Fig. 6B). The maximum activity of HnpAB for 2,6-DCNP was 0.42 ± 0.07 U mg^{-1}. The enzymatic kinetic assays revealed that HnpAB transformed 2,6-DCNP with a K_m of 3.9 ± 1.4 μM and a k_{cat}/K_m of 0.12 ± 0.04 μM^{-1} min^{-1}.

Two compounds with GC retention times of 9.87 and 10.74 min, respectively, were detected by the GC-MS analysis of the acetylated products of 2,6-DCNP catalyzed by the purified HnpAB. The mass spectrum of the product at 9.87 min showing the typical fragmentation pattern of 2,6-dichlorohydroquinone (2,6-DCHQ) (Louie et al., 2002), with a molecular ion peak at *m/z* 262.04 and the fragments at *m/z* 219.94 (losing one acetyl group) and *m/z* 177.96 (losing two acetyl groups) (Fig. 6C). The mass spectrum of the product at 10.74 min showing the typical fragmentation pattern of acetylated 6-chlorohydroxyquinol (6-CHQ), which showed a molecular ion peak at *m/z* 286.04 as well as the fragments at *m/z* 244.05 (losing one acetyl group), 201.97 (losing two acetyl groups) and 159.97 (losing three acetyl groups) (Fig. 6D). In addition to 2,6-DCNP, the purified HnpAB is also able to catalyze the conversion of 2,6-DCHQ to 6-CHQ in the presence of NADH and FAD, although with a very slow rate of 0.005 ± 0.0028 U mg^{-1}.

3.6. *hnpA* plays a crucial role in 2,6-DCNP catabolism in CNP-8

Strains CNP-8Δ*hnpA* and CNP-8Δ*hnpA*[pRK-*hnpA*] (Table S1), the *hnpA* deleted and complemented derivatives of strains CNP-8 were constructed to investigate the physiological role of HnpA in the catabolism of 2,6-DCNP. Strain CNP-8Δ*hnpA* completely lost the ability to grow on 2,6-DCNP, whereas strain CNP-8Δ*hnpA*[pRK-*hnpA*] recovered the ability to utilize 2,6-DCNP (Fig. S5). This indicated that *hnpA1* plays a crucial role in 2,6-DCNP catabolism.

3.7. The evolutionary origin of HnpA

To elucidate the phylogenetic origin of HnpA, members of the oxygenase components of the two component aromatic monooxygenases were selected to construct the distance neighbor-joining tree. As shown in Fig. 7, the phylogenetic tree is divided into two larger branches. HnpA located in the upper branch that mainly contains the phenol *para*-position monooxygenases including the functionally identified *para*-nitrophenol monooxygenases NpcA (Kitagawa et al., 2004) and NpdA2 (Perry and Zylstra, 2007; Liu et al., 2010), 2-chloro-4-nitrophenol and *para*-nitrophenol monooxygenase PnpA1 (Min et al., 2016), 2,4,5-trichlorophenol (2,4,5-TCP) monooxygenase TftD (Hubner et al., 1998) and 2,4,6-trichlorophenol (2,4,6-TCP) monooxygenases TcpA (Xun and Webster, 2004). The lower branch mainly contains the phenol *ortho*-position monooxygenases including the

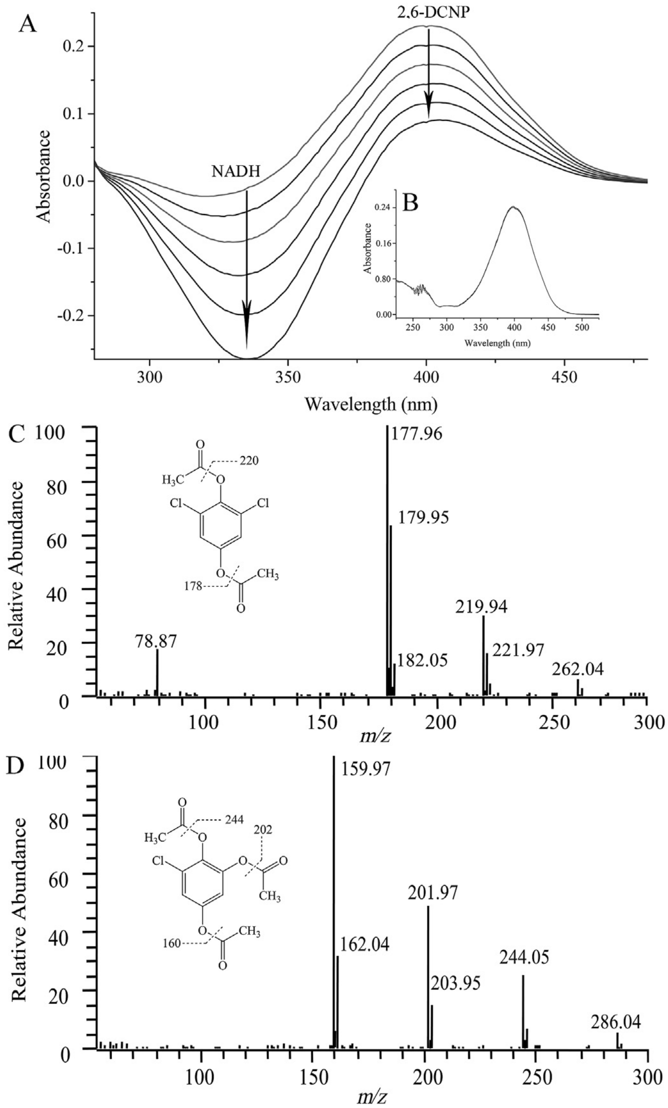

Fig. 6. Enzymatic activity assay of HnpAB against 2,6-DCNP, together with the products identification. (A) Spectral changes during the transformation of 2,6-CBNP by purified HnpAB. (B) Spectral changes during the transformation of 2,6-CBNP by only purified HnpA. (C) The mass spectra of acetylated 2,6-DCHQ. (D) The mass spectra of acetylated 6-CHQ.

functionally identified PNP monooxygenase NphA1 (Takeo et al., 2008), 4-hydroxyphenylacetate monooxygenase HpaB (Galan et al., 2000) and phenol monooxygenase PheA1 (Duffner et al., 2000; Kirchner et al., 2003). In the phenol *para*-position monooxygenases branch, HnpA is closely related to chlorophenol monooxygenases (such as TftD, HadA and TcpA) but distantly related to nitrophenol monooxygenases (such as NpcA, NpdA2 and PnpA1).

4. Discussion

2,6-DCNP is an emerging chlorinated nitroaromatic pollutant and has been widely introduced into our surrounding environment (Xiao et al., 2012). To date, nevertheless, no microorganism has been reported to degrade 2,6-DCNP, not to mention the degradation kinetics, catabolic pathway and molecular mechanism information. Herein, *Cupriavidus* sp. strain CNP-8, previously reported to degrade various nitrophenols (Min et al., 2017b, 2018; 2019) was found to be also able to utilize 2,6-DCNP as the sole source of carbon and nitrogen, and remove two chlorines from 2,6-DCNP (Fig. 1). The degradation kinetics of 2,6-DCNP (Fig. 2), together with simultaneous removal of mixture CNPs by this strain (Fig. 3) indicated that strain CNP-8 is an efficient candidate for bioremediation. Moreover, this study provides biochemical and molecular information for microbial 2,6-DCNP degradation, filling the gap in our understanding of its fate in the environment.

The investigation of degradation kinetics showed that strain CNP-8 degraded 2,6-DCNP less than 1.0 mM, with μ_{max} of 0.124 h^{-1}, q_{max} of 0.217 mg mg^{-1} h^{-1}, K_s of 0.038 mM and K_i of 0.42 mM (Fig. 2 and Fig. S2). These kinetic parameters are very important in assessing the ability and limitation of strain CNP-8 during biodegradation (Shen et al., 2009; Tiwari et al., 2017). Because strain CNP-8 is the first bacterium with the ability to degrade 2,6-DCNP, the knowledge of microbial degradation kinetics of 2,6-DCNP is unavailable in the literature. Thus, we are unable to compare 2,6-DCNP degradation efficiency between strain CNP-8 and other bacteria. Although strain CNP-8 could utilize 2,6-DCNP, the bacterial growth was inhibited by high concentration substrate (Fig. S1). Therefore, the Haldane's model which is widely application in describing the bacterial growth kinetics against inhibitory aromatics (Shen et al., 2009; Zhang et al., 2009a,b; Sahoo et al., 2011a), was used to investigate the microbial degradation kinetics of 2,6-DCNP. Fig. 2 showed that the maximum specific growth rate occurred at low 2,6-DCNP concentration; further increasing substrate concentration resulted in the decline of the specific growth rate, in line with the variation tendency of the maximum specific degradation rates (Fig. S2). This phenomenon is in accord with the microbial degradation of many aromatic compounds such as phenol (Wang et al., 2010), 4-chlorophenol (Sahoo et al., 2011a), 4-nitrophenol (Sahoo et al., 2011b), 2C4NP (Min et al., 2018) and 2,4,6-trinitrophenol (Shen et al., 2009). When strain CNP-8 grown on 2,6-DCNP at different concentration, the biomass yield coefficient reached the highest value when initial 2,6-DCNP concentration is 0.2 mM, and further increase substrate concentration resulted in the significant decrease of biomass yield coefficient (Fig. S3). The significant decrease of biomass yield coefficient at high 2,6-DCNP concentration indicated that more energy resulting from substrate degradation was required to overcome the 2,6-DCNP inhibition against strain CNP-8. This hypothesis has also been proposed previously to explain the microbial degradation of many toxic xenobiotics (Shen et al., 2009; Wang et al., 2010; Sahoo et al., 2011a; Min et al., 2018; Min et al., 2019). In summary, although the inhibition effect of 2,6-DCNP against CNP-8 was inevitable, the extremely lower value of K_s (0.03 mM) than that of K_i (0.42 mM) indicated that CNP-8 was able to effectively remove 2,6-DCNP from the point of kinetic view.

Biotransformation assays showed that either 2,6-DCNP- or 2,6-DBNP-induced cells of strain CNP-8 have the ability to degrade both 2,6-DCNP and 2,6-DBNP rapidly (Fig. 4). Moreover, the transcriptional level of *hnp* genes increased significantly after induction by the substrate (Fig. 5B). These indicated that the *hnp* cluster was also responsible for the catabolism of 2,6-DCNP, in addition to degrading 2,6-DBNP. To date, limited literature reported that bacterium degraded different halogenated nitroaromatics by the enzymes encoded by the same gene cluster. Recently, *Pseudomonas stutzeri* ZWLR2-1, a 2-chloronitrobenzene (2CNB) and 2-bromonitrobenzene (2BNB) utilizer, was reported to degrade 2CNB and 2BNB by the enzymes encoded by the same *cnb* gene cluster (Liu et al., 2011; Wang et al., 2019). This study yet provides another example of a bacterium using the same set of enzymes to degrade multiple substrates, making the *hnp* cluster well adapted for bioremediation of various halogenated nitrophenols-contaminated environments.

The function of HnpAB was experimentally validated both

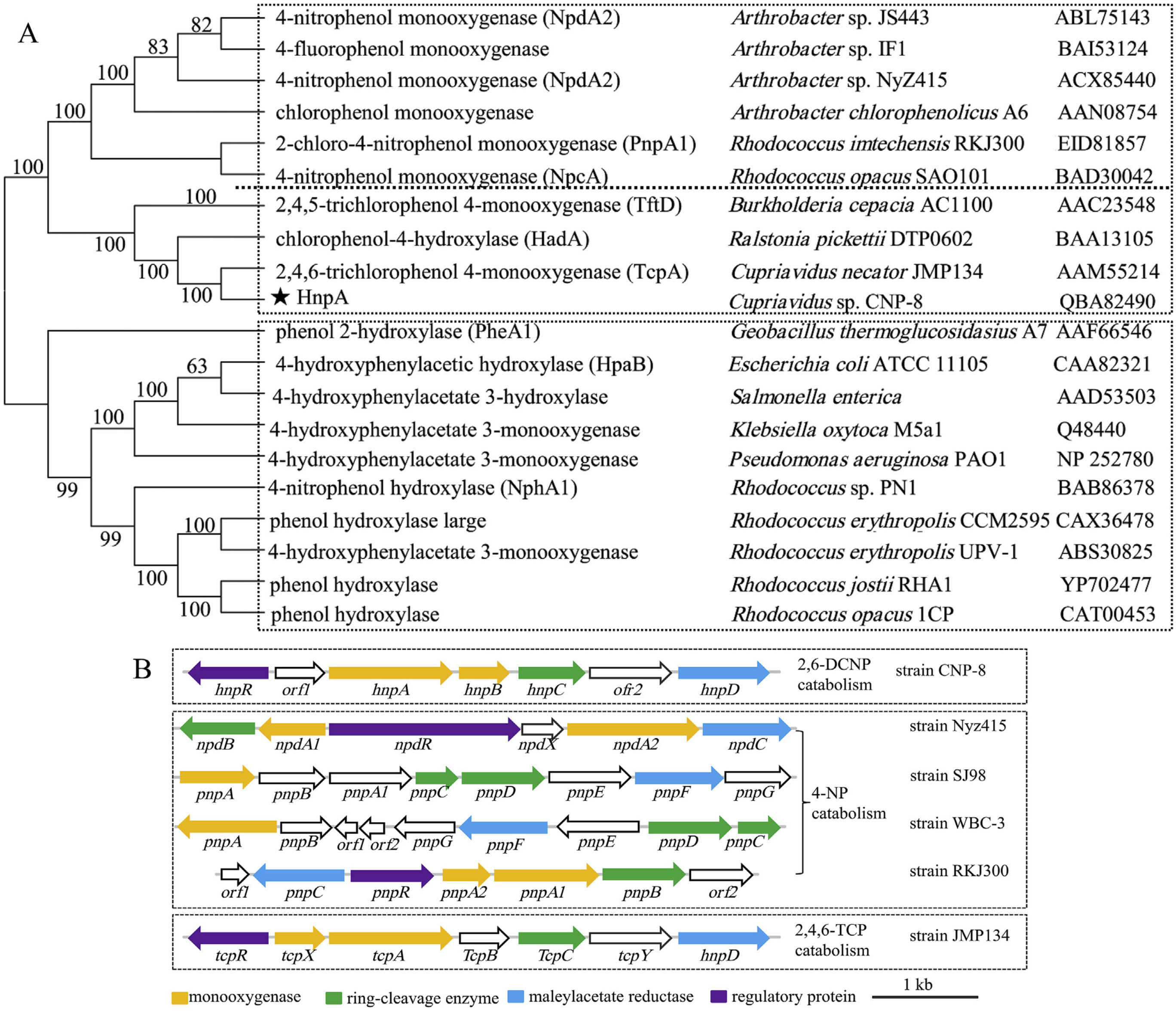

Fig. 7. (A) Phylogenetic relationship of the oxygenase component of the two-component phenols monooxygenases including HnpA. HnpA is indicated by a "★". (B) Comparison of the genetic organization of the *hnp* gene cluster involved in 2,6-DCNP catabolism in strain CNP-8, the *tcp* gene cluster involved in 2,4,6-TCP catabolism in *Cuptiavidus necator* JMP134 and the gene clusters involved in 4-nitrophenol catabolism in some bacteria.

in vitro (Fig. 6) and *in vivo* (Fig. S5). Enzymatic assay showed that the purified HnpAB catalyzed the transformation of 2,6-DCNP rapidly, together with the formation of 2,6-DCHQ and 6-CHQ (Fig. 6). The identification of 2,6-DCHQ and 6-CHQ indicated that this two-component monooxygenase has the ability to catalyze the sequential denitration and dechlorination of 2,6-DCNP. It is well accepted that monooxygenases attack the phenolic ring substituted with chloro or nitro generating quinone compounds (Xun and Webster, 2004; Perry and Zylstra, 2007; Min et al., 2016). Therefore, the identification of 2,6-DCHQ indicated that 2,6-dichloro-1, 4-benzoquinone (2,6-DCBQ) was the actual product of 2,6-DCNP catalyzed by HnpAB (Fig. 8). Several analysis method including HPLC and GC-MS were used to identify 2,6-DCBQ, but failed after many attempts. This is due to that 2,6-DCBQ was rapidly reduced 2,6-DCHQ by NADH in the enzyme reaction system, which can be justified by numerous reports revealing that (chlorinated) quinones would be rapidly reduced to the corresponding (chlorinated) phenols in the presence of NADH (Xun and Webster, 2004; Perry and Zylstra, 2007; Liu et al., 2010; Min et al., 2016; Min et al., 2019). In addition to catalyzing 2,6-DCNP degradation, the purified HnpAB also catalyzed the conversion of 2,6-DCHQ to 6-CHQ (Fig. 8), similar with the catalytic activity of its counterparts (TcpAX) against 2,6-DCHQ during 2,4,6-TCP degradation by *Cupriavidus necator* JMP134 (Louie et al., 2002; Belchik and Xun, 2008). Therefore, during the catabolism of 2,6-DCNP *in vivo*, the toxicity of potential by-product 2,6-DCHQ against the cells could be eliminated by the transformation of 2,6-DCHQ to 6-CHQ. On the other hand, the identification of 6-CHQ presented strong evidence that 2,6-DCBQ would be further hydroxylated to 6-CHQ via 6-chlorohydroxyquinone by HnpAB (Fig. 8). Indeed, most $FADH_2$-dependent monooxygenases have been reported to hydroxylate their substrates twice in tandem (Louie et al., 2002; Xun and Webster, 2004; Min et al., 2016; Pimviriyakul et al., 2017).

Generally, the genes responsible for catabolism of nitroaromatic

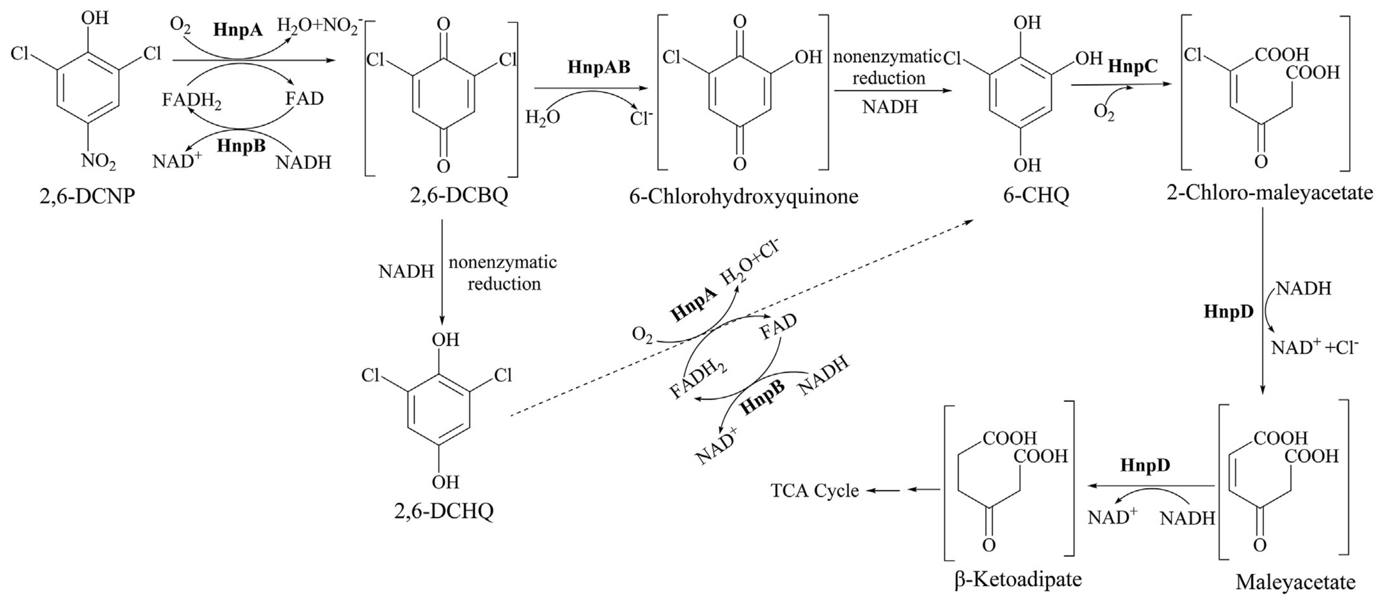

Fig. 8. The catabolic pathway of 2,6-DCNP in *Cupriavidus* sp. strain CNP-8. TCA, tricarboxylic acid. The unidentified intermediate is in bracket.

compounds are clustered in the genome. In this strain, *hnpC* and *hnpD* genes are clustered with *hnpA*, which is necessary for strain CNP-8 to utilize 2,6-DBNP (Fig. S5). Moreover, transcriptional level by RT-qPCR showed that both *hnpC* and *hnpD* are up-regulated by 2,6-DCNP induction. These indicated HnpC and HnpD are involved in the catabolism of 2,6-DCNP. The catalytic activity of HnpC and HnpD was not performed because the commercial substrates are unavailable. However, considering that HnpC exhibited very high identity (93%) with the 6-CHQ dioxygenase (TcpC) from *Cupriavidus necator* JMP134, which was experimentally validated to transform 6-CHQ to 2-chloromaleylacetate (2-BMA) (Louie et al., 2002); therefore, HnpC is likely responsible for ring-cleavage of 6-CHQ to 2-chloromaleylacetate (2-CMA) during 2,6-DCNP degradation in strain CNP-8 (Fig. 8). HnpD is a maleylacetate reductase. Previously, many maleylacetate reductases were reported to be able to catalyze the dechlorination of 2-CMA to maleylacetate (MA), followed by transform MA to β-ketoadipate (Kaschabek and Reineke, 1995; Min et al., 2014). Therefore, HnpD likely transform 2-CMA twice in tandem, with the formation of β-ketoadipate during the catabolism of 2,6-DCNP (Fig. 8).

The enzymatic assay and product identification indicated that HnpAB catalyzed the sequential *para*- and *ortho*-position hydroxylation of 2,6-DCNP. However, the phylogenetic analysis (Fig. 7A) showed that HnpA is closely related to the phenols *para*-monooxygenases (Hubner et al., 1998; Xun and Webster, 2004; Perry and Zylstra, 2007; Liu et al., 2010; Min et al., 2016), but distantly related to the phenols *ortho*-monooxygenases (Duffner et al., 2000; Galan et al., 2000; Kirchner et al., 2003; Takeo et al., 2008). In the phenols *para*-monooxygenases family, HnpA is more closely related to the chlorophenols monooxygenases such as 2,4,5-TCP monooxygenase (Hubner et al., 1998) and 2,4,6-TCP monooxygenase (Xun and Webster, 2004) than the nitrophenols monooxygenases such as the 4-nitrophenol monooxygenases (Perry and Zylstra, 2007; Liu et al., 2010; Min et al., 2016). Furthermore, the genetic organization of *hnp* cluster in strain CNP-8 was similar with that of the *tcp* cluster involved in 2,4,6-TCP catabolism in *Cuptiavidus necator* JMP134 (Louie et al., 2002), but significantly different from those of the clusters involved in the catabolism of 4-nitrophenols in several bacteria (Fig. 7B) (Zhang et al., 2009a,b; Liu et al., 2010; Min et al., 2014; Min et al., 2016). These indicated that the *hnp* cluster responsible for the catabolism of halogenated nitrophenols (2,6,-DCNP and 2,6,-DBNP) in strain CNP-8 originated from the cluster involved in the catabolism of chlorophenols rather than nitrophenols.

5. Conclusions

We reports the microbial degradation of 2,6-DCNP for the first time. The biodegradation kinetics of 2,6-DCNP was investigated by strain CNP-8. The two-component monooxygenase HnpAB catalyzes the denitration and dechlorination of 2,6-DCNP twice in tandem. The phylogenetic analysis indicated that the *hnp* cluster originated from the cluster involved in the catabolism of chlorophenols rather than nitrophenols. This study fills a gap in our knowledge of the microbial 2,6-DCNP degradation.

Author contributions

J. M. and X. H. designed the experiment, J. M. and L. X. performed the experiment, J. M., S. F, and W. C. analyzed data, J. M., and X. H. wrote the paper.

Declaration of competing interest

The authors declare no competing financial interest.

Acknowledgements

This work was supported by the National Natural Science Foundation of China (No. 31600085), the State's Key Project of Research and Development Plan (2016YFC1402300), the Foreword Key Priority Research Program of Chinese Academy of Sciences (QYZDB-SSW-DQC013), the Youth Innovation Promotion Association Program of the Chinese Academy of Sciences to Dr. Jun Min, and the Yantai Science and Technology Project (2017ZH092).

Appendix A. Supplementary data

Supplementary data to this article can be found online at https://doi.org/10.1016/j.envpol.2019.113703.

References

Ahmadi, E., Gholami, M., Farzadkia, M., Nabizadeh, R., Azari, A., 2015. Study of moving bed biofilm reactor in diethyl phthalate and diallyl phthalate removal from synthetic wastewater. Bioresour. Technol. 183, 129–135.

Arora, P.K., Jain, R.K., 2011. Pathway for degradation of 2-chloro-4-nitrophenol in *Arthrobacter* sp. SJCon. Curr. Microbiol. 63, 568–573.

Arora, P.K., Jain, R.K., 2012. Metabolism of 2-chloro-4-nitrophenol in a gram negative bacterium, *Burkholderia* sp. RKJ 800. PLoS One 7.

Arora, P.K., Sasikala, C., Ramana Ch, V., 2012a. Degradation of chlorinated nitroaromatic compounds. Appl. Microbiol. Biotechnol. 93, 2265–2277.

Arora, P.K., Sharma, A., Mehta, R., Shenoy, B.D., Srivastava, A., Singh, V.P., 2012b. Metabolism of 4-chloro-2-nitrophenol in a gram-positive bacterium, *Exiguobacterium sp.* PMA. Microb. Cell. Fact. 11, 150.

Arora, P.K., Srivastava, A., Garg, S.K., Singh, V.P., 2018. Recent advances in degradation of chloronitrophenols. Bioresour. Technol. 250, 902–909.

Arora, P.K., Srivastava, A., Singh, V.P., 2014. Degradation of 4-chloro-3-nitrophenol via a novel intermediate, 4-chlororesorcinol by *Pseudomonas* sp. JHN. Sci. Rep. 4, 4475.

Belchik, S.M., Xun, L.Y., 2008. Functions of flavin reductase and quinone reductase in 2,4,6-trichlorophenol degradation by *Cupriavidus necator* JMP134. J. Bacteriol. 190, 1615–1619.

Bradford, M.M., 1976. A rapid and sensitive method for the quantitation of microgram quantities of protein utilizing the principle of protein-dye binding. Anal. Biochem. 72, 248–254.

Chen, Y.F., Chao, H., Zhou, N.Y., 2014. The catabolism of 2,4-xylenol and *p*-cresol share the enzymes for the oxidation of *para*-methyl group in *Pseudomonas putida* NCIMB 9866. Appl. Microbiol. Biotechnol. 98, 1349–1356.

Cunliffe, M., Kertesz, M.A., 2006. Effect of Sphingobium yanoikuyae B1 inoculation on bacterial community dynamics and polycyclic aromatic hydrocarbon degradation in aged and freshly PAH-contaminated soils. Environ. Pollut. 144, 228–237.

Chi, X.Q., Zhang, J.J., Zhao, S., Zhou, N.Y., 2013. Bioaugmentation with a consortium of bacterial nitrophenol-degraders for remediation of soil contaminated with three nitrophenol isomers. Environ. Pollut. 172, 33–41.

Dastgheib, S.M., Amoozegar, M.A., Khajeh, K., Shavandi, M., Ventosa, A., 2012. Biodegradation of polycyclic aromatic hydrocarbons by a halophilic microbial consortium. Appl. Microbiol. Biotechnol. 95, 789–798.

Duffner, F.M., Kirchner, U., Bauer, M.P., Muller, R., 2000. Phenol/cresol degradation by the thermophilic *Bacillus thermoglucosidasius* A7: cloning and sequence analysis of five genes involved in the pathway. Gene 256, 215–221.

Fu, H., Zhang, J.J., Xu, Y., Chao, H.J., Zhou, N.Y., 2017. Simultaneous biodegradation of three mononitrophenol isomers by a tailor-made microbial consortium immobilized in sequential batch reactors. Lett. Appl. Microbiol. 64, 203–209.

Galan, B., Diaz, E., Prieto, M.A., Garcia, J.L., 2000. Functional analysis of the small component of the 4-hydroxyphenylacetate 3-monooxygenase of *Escherichia coli* W: a prototype of a new flavin : NAD(P)H reductase subfamily. J. Bacteriol. 182, 627–636.

Ghosh, A., Khurana, M., Chauhan, A., Takeo, M., Chakraborti, A.K., Jain, R.K., 2010. Degradation of 4-nitrophenol, 2-chloro-4-nitrophenol, and 2,4-dinitrophenol by *Rhodococcus imtechensis* strain RKJ300. Environ. Sci. Technol. 44, 1069–1077.

Hubner, A., Danganan, C.E., Xun, L., Chakrabarty, A.M., Hendrickson, W., 1998. Genes for 2,4,5-trichlorophenoxyacetic acid metabolism in *Burkholderia cepacia* AC1100: characterization of the *tftC* and *tftD* genes and locations of the *tft* operons on multiple replicons. Appl. Environ. Microbiol. 64, 2086–2093.

Jiang, J.Y., Zhang, X.R., Zhu, X.H., Li, Y., 2017. Removal of intermediate aromatic halogenated DBPs by activated carbon adsorption: a new approach to controlling halogenated DBPs in chlorinated drinking water. Environ. Sci. Technol. 51, 3435–3444.

Kaschabek, S.R., Reineke, W., 1995. Maleylacetate reductase of *Pseudomonas* sp. strain B13: specificity of substrate conversion and halide elimination. J. Bacteriol. 177, 320–325.

Kirchner, U., Westphal, A.H., Muller, R., van Berkel, W.J., 2003. Phenol hydroxylase from *Bacillus thermoglucosidasius* A7, a two-protein component monooxygenase with a dual role for FAD. J. Biol. Chem. 278, 47545–47553.

Kitagawa, W., Kimura, N., Kamagata, Y., 2004. A novel p-nitrophenol degradation gene cluster from a gram-positive bacterium, *Rhodococcus opacus* SAO101. J. Bacteriol. 186, 4894–4902.

Lessner, D.J., Johnson, G.R., Parales, R.E., Spain, J.C., Gibson, D.T., 2002. Molecular characterization and substrate specificity of nitrobenzene dioxygenase from *Comamonas* sp. strain JS765. Appl. Environ. Microbiol. 68, 634–641.

Liu, H., Wang, S.J., Zhou, N.Y., 2005. A new isolate of *Pseudomonas stutzerithat* degrades 2-chloronitrobenzene. Biotechnol. Lett. 27, 275–278.

Liu, H., Wang, S.J., Zhang, J.J., Dai, H., Tang, H., Zhou, N.Y., 2011. Patchwork assembly of *nag*-like nitroarene dioxygenase genes and the 3-chlorocatechol degradation cluster for evolution of the 2-chloronitrobenzene catabolism pathway in *Pseudomonas stutzeri* ZWLR2-1. Appl. Environ. Microbiol. 77, 4547–4552.

Liu, J.Q., Zhang, X.R., 2014. Comparative toxicity of new halophenolic DBPs in chlorinated saline wastewater effluents against a marine alga: halophenolic DBPs are generally more toxic than haloaliphatic ones. Water Res. 65, 64–72.

Liu, J.Q., Zhang, X.R., Li, Y., Li, W.X., Hang, C., Sharma, V.K., 2019. Phototransformation of halophenolic disinfection byproducts in receiving seawater: kinetics, products, and toxicity. Water Res. 150, 68–76.

Liu, P.-P., Zhang, J.-J., Zhou, N.-Y., 2010. Characterization and mutagenesis of a two-component monooxygenase involved in para-nitrophenol degradation by an Arthrobacter strain. Int. Biodeterior. Biodegrad. 64, 293–299.

Livak, K.J., Schmittgen, T.D., 2001. Analysis of relative gene expression data using real-time quantitative PCR and the $2^{-\Delta\Delta CT}$ method. Methods 25, 402–408.

Louie, T.M., Webster, C.M., Xun, L., 2002. Genetic and biochemical characterization of a 2,4,6-trichlorophenol degradation pathway in *Ralstonia eutropha* JMP134. J. Bacteriol. 184, 3492–3500.

Min, J., Chen, W., Hu, X., 2019. Biodegradation of 2,6-dibromo-4-nitrophenol by *Cupriavidus* sp. strain CNP-8: kinetics, pathway, genetic and biochemical characterization. J. Hazard Mater. 361, 10–18.

Min, J., Chen, W., Wang, J., Hu, X., 2017b. Genetic and biochemical characterization of 2-chloro-5-nitrophenol degradation in a newly isolated bacterium, *Cupriavidus* sp. strain CNP-8. Front. Microbiol. 8, 1778.

Min, J., Wang, B., Hu, X., 2017a. Effect of inoculation of *Burkholderia* sp. strain SJ98 on bacterial community dynamics and *para*-nitrophenol, 3-methyl-4-nitrophenol, and 2-chloro-4-nitrophenol degradation in soil. Sci. Rep. 7, 5983.

Min, J., Wang, J., Chen, W., Hu, X., 2018. Biodegradation of 2-chloro-4-nitrophenol via a hydroxyquinol pathway by a Gram-negative bacterium, *Cupriavidus* sp. strain CNP-8. AMB Express 8, 43.

Min, J., Zhang, J.J., Zhou, N.Y., 2014. The gene cluster for *para*-nitrophenol catabolism is responsible for 2-chloro-4-nitrophenol degradation in *Burkholderia* sp. strain SJ98. Appl. Environ. Microbiol. 80, 6212–6222.

Min, J., Zhang, J.J., Zhou, N.Y., 2016. A two-component *para*-nitrophenol monooxygenase initiates a novel 2-chloro-4-nitrophenol catabolism pathway in *Rhodococcus imtechensis* RKJ300. Appl. Environ. Microbiol. 82, 714–723.

Niu, G.L., Zhang, J.J., Zhao, S., Liu, H., Boon, N., Zhou, N.Y., 2009. Bioaugmentation of a 4-chloronitrobenzene contaminated soil with *Pseudomonas putida* ZWL73. Environ. Pollut. 157, 763–771.

Pandey, J., Heipieper, H.J., Chauhan, A., Arora, P.K., Prakash, D., Takeo, M., et al., 2011. Reductive dehalogenation mediated initiation of aerobic degradation of 2-chloro-4-nitrophenol (2C4NP) by *Burkholderia* sp. strain SJ98. Appl. Microbiol. Biotechnol. 92, 597–607.

Pimviriyakul, P., Thotsaporn, K., Sucharitakul, J., Chaiyen, P., 2017. Kinetic mechanism of the dechlorinating flavin-dependent monooxygenase HadA. J. Biol. Chem. 292, 4818–4832.

Perry, L.L., Zylstra, G.J., 2007. Cloning of a gene cluster involved in the catabolism of *p*-nitrophenol by *Arthrobacter* sp. strain JS443 and characterization of the *p*-nitrophenol monooxygenase. J. Bacteriol. 189, 7563–7572.

Sahoo, N.K., Pakshirajan, K., Ghosh, P.K., Ghosh, A., 2011a. Biodegradation of 4-chlorophenol by *Arthrobacter chlorophenolicus* A6: effect of culture conditions and degradation kinetics. Biodegradation 22, 275–286.

Sahoo, N.K., Pakshirajan, K., Ghosh, P.K., 2011b. Batch biodegradation of *para*-nitrophenol using *Arthrobacter chlorophenolicus* A6. Appl. Biochem. Biotechnol. 165, 1587–1596.

Schenzle, A., Lenke, H., Spain, J.C., Knackmuss, H.J., 1999. Chemoselective nitro group reduction and reductive dechlorination initiate degradation of 2-chloro-5-nitrophenol by *Ralstonia eutropha* JMP134. Appl. Environ. Microbiol. 65, 2317–2323.

Shen, J., He, R., Wang, L., Zhang, J., Zuo, Y., Li, Y., et al., 2009. Biodegradation kinetics of picric acid by *Rhodococcus* sp.NJUST16 in batch reactors. J. Hazard Mater. 167, 193–198.

Sun, Y., Qiu, J., Chen, D., Ye, J., Chen, J., 2016. Characterization of the novel dimethyl sulfide-degrading bacterium *Alcaligenes* sp. SY1 and its biochemical degradation pathway. J. Hazard Mater. 304, 543–552.

Takeo, M., Murakami, M., Niihara, S., Yamamoto, K., Nishimura, M., Kato, D., et al., 2008. Mechanism of 4-nitrophenol oxidation in *Rhodococcus* sp. strain PN1: characterization of the two-component 4-nitrophenol hydroxylase and regulation of its expression. J. Bacteriol. 190, 7367–7374.

Tamura, K., Peterson, D., Peterson, N., Stecher, G., Nei, M., Kumar, S., 2011. MEGA5: molecular evolutionary genetics analysis using maximum likelihood, evolutionary distance, and maximum parsimony methods. Mol. Biol. Evol. 28, 2731–2739.

Tiwari, J., Naoghare, P., Sivanesan, S., Bafana, A., 2017. Biodegradation and detoxification of chloronitroaromatic pollutant by *Cupriavidus*. Bioresour. Technol. 223, 184–191.

Wang, L., Chi, X.Q., Zhang, J.J., Sun, D.L., Zhou, N.Y., 2014. Bioaugmentation of a methyl parathion contaminated soil with *Pseudomonas* sp. strain WBC-3. Int. Biodeterior. Biodegrad. 87, 116–121.

Wang, L.M., Li, Y., Yu, P., Xie, Z.X., Luo, Y.B., Lin, Y.W., 2010. Biodegradation of phenol at high concentration by a novel fungal strain *Paecilomyces variotii* JH6. J. Hazard Mater. 183, 366–371.

Wang, L., Gao, Y.Z., Zhao, H., Xu, Y., Zhou, N.Y., 2019. Biodegradation of 2-bromonitrobenzene by *Pseudomonas stutzeri* ZWLR2-1. Int. Biodeterior. Biodegrad. 138, 87–91.

Xiao, F., Zhang, X., Zhai, H., Lo, I.M., Tipoe, G.L., Yang, M., et al., 2012. New halogenated disinfection byproducts in swimming pool water and their permeability across skin. Environ. Sci. Technol. 46, 7112–7119.

Xun, L.Y., Webster, C.M., 2004. A monooxygenase catalyzes sequential dechlorinations of 2,4,6-trichlorophenol by oxidative and hydrolytic reactions. J. Biol. Chem. 279, 6696–6700.

Yang, M., Zhang, X., 2013. Comparative developmental toxicity of new aromatic halogenated DBPs in a chlorinated saline sewage effluent to the marine polychaete Platynereis dumerilii. Environ. Sci. Technol. 47, 10868–10876.

Yue, W., Chen, M., Cheng, Z., Xie, L., Li, M., 2018. Bioaugmentation of strain *Methylobacterium* sp. C1 towards *p*-nitrophenol removal with broad spectrum

coaggregating bacteria in sequencing batch biofilm reactors. J. Hazard Mater. 344, 431–440.
Zhang, J., Sun, Z., Li, Y., Peng, X., Li, W., Yan, Y., 2009a. Biodegradation of *p*-nitrophenol by *Rhodococcus* sp. CN6 with high cell surface hydrophobicity. J. Hazard Mater. 163, 723–728.
Zhang, J.J., Liu, H., Xiao, Y., Zhang, X.E., Zhou, N.Y., 2009b. Identification and characterization of catabolic *para*-nitrophenol 4-monooxygenase and *para*-benzoquinone reductase from *Pseudomonas* sp. strain WBC-3. J. Bacteriol. 191, 2703–2710.